ATMOSPHERIC SCIENCE

# Mesoscale convective clustering enhances tropical precipitation

**Pedro Angulo-Umana and Daehyun Kim***



**In the tropics, extreme precipitation events are often caused by mesoscale systems of organized, spatially clustered deep cumulonimbi, posing a substantial risk to life and property. While the clustering of convective clouds has been thought to strengthen precipitation rate, no quantitative estimates of this hypothesized enhancement exist. In this study, after isolating the effects of mesoscale convective clustering on precipitation, we find that strongly clustered oceanic convection precipitates more intensely than weakly clustered convection. We further show that this enhancement is primarily attributable to an increase in convective precipitation rate when the environment is less than 70% saturated, with increases in the size of the rainy stratiform region being of equal or greater importance when the environment is closer to saturation. Our results suggest that a correct representation of mesoscale organized convective systems in numerical weather and climate models is needed for accurate predictions of extreme precipitation events.**

## INTRODUCTION

Tropical convection organizes into coherent structures exhibiting a wide range of spatial and temporal scales. Examples of organized tropical convective systems include mesoscale convective systems (*1*), tropical cyclones, and the Madden-Julian Oscillation (*2*). Among these organized systems, mesoscale systems of clustered convection are of first-order importance to the tropical hydrological cycle; they produce more than 60% of the total precipitation in the tropics (*3*, *4*) and are the main drivers of extreme precipitation events (*5*–*7*). Moreover, changes in the frequency of mesoscale organized convective systems have been ascribed as the cause of changes in tropical rainfall patterns observed in recent decades (*8*) and have been suggested as a potential cause of the future changes to global precipitation patterns predicted in simulations of greenhouse gas–induced global warming (*9*, *10*). Unfortunately, these organized convective systems remain poorly represented in most numerical models for weather and climate prediction (*11*, *12*), making it difficult to accurately simulate tropical precipitation or predict how tropical precipitation will change with global warming. One bottleneck for efforts seeking to improve the representation of mesoscale systems of clustered convection in models is the lack of observational constraints on the nature of those systems.

One such constraint that is presently absent from the literature is a quantitative measure of the effect that mesoscale convective organization, as well as its associated clustering of precipitating cumulus clouds, has on precipitation rate. While previous studies have argued—on the basis of observational data, model output, and heuristic reasoning—that clustered convection should precipitate more intensely than nonclustered convection, no estimate of the enhancement of precipitation rate that can be attributed to a stronger degree of convective clustering presently exists. This study seeks to quantify and diagnose the changes in precipitation rate over mesoscale domains associated with a stronger degree of clustering of convective clouds.

Department of Atmospheric Sciences, University of Washington, Seattle, WA, USA.
*Corresponding author. Email: daehyun@uw.edu

## RESULTS

### Convective clustering enhances precipitation

Tropical precipitation has been observed to depend very strongly on two quantities in particular: convective area fraction (CAF) (*13*–*16*), defined as the areal fraction of the domain in question that is undergoing convection, and saturation fraction (SF) (*17*–*21*), also termed column relative humidity, defined as the vertically integrated vapor content of the domain normalized by the saturation capacity of the domain. Therefore, to estimate the response of tropical precipitation to an enhanced degree of convective clustering, we need to stratify our data to compare cases that differ primarily in their degree of mesoscale clustering but are similar in terms of CAF and SF.

The SF values of scenes are obtained from the fifth-generation European Centre for Medium-Range Weather Forecasts (ECMWF) reanalysis product (ERA5) (*22*). The averaged surface rain rate, CAF, and degree of spatial clustering of the convection are obtained from the NASA Tropical Rainfall Measuring Mission (TRMM) Precipitation Radar (PR) dataset (see Materials and Methods). These data provide snapshots of gridded estimated surface rain rate, as well as rain type classification, allowing for the identification of which rainy pixels are undergoing convective precipitation (see Materials and Methods). Because our focus is on mesoscale convective clustering, we segment these snapshots into smaller domains, which we call scenes. We consider 1° × 1°, 2° × 2°, and 3° × 3° scenes to test the sensitivity of our results to the size of domain being analyzed. Figure 1 shows examples of rain rate and rain type data for 2° × 2° scenes. As in many recent studies (*13*, *23*–*26*), we quantify the degree of convective clustering present in a scene by the organization index ($I_{org}$), which is larger for more strongly clustered scenes (*24*). TRMM rain type data are used to compute $I_{org}$ for each scene (see Materials and Methods). Some previous studies examining the relationship between convective clustering and precipitation have used precipitation thresholds to identify deep convection [e.g., (*13*)]. To test the robustness of our results, $I_{org}$ is computed both with and without rain rate thresholds (see Materials and Methods). We additionally compute $I_{org}$ both with and without the grouping of adjacent convective pixels (see

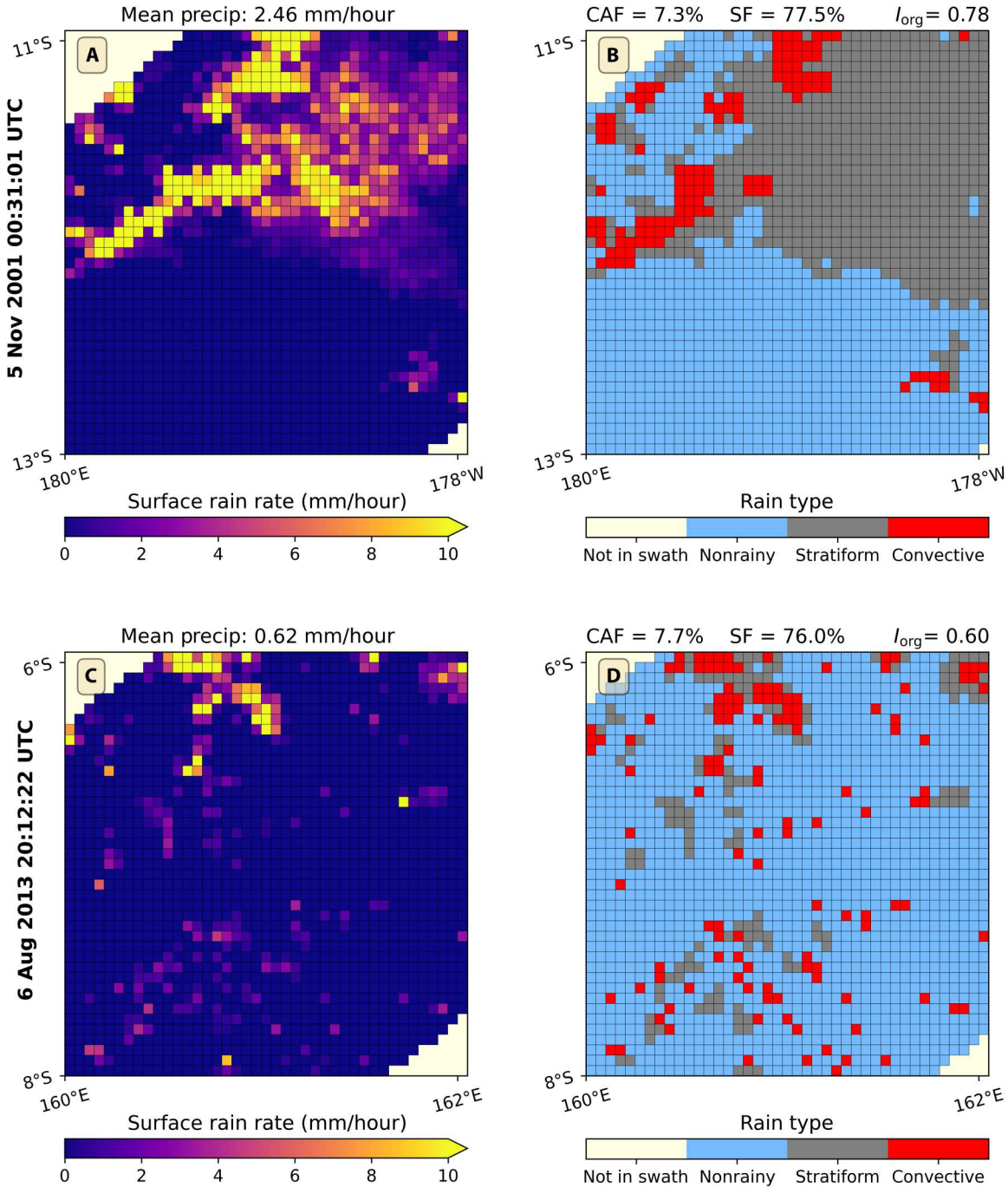


**Fig. 1. Examples of scenes.** Two scenes are shown above, with similar SF and CAF but differing precipitation intensities and degrees of convective clustering. Scene 1 (**A** and **B**) was observed on 5 November 2001 at 00:31:01 UTC and has latitudinal extent from 13°S to 11°S and longitudinal extent from 180°E to 178°W. Scene 2 (**C** and **D**) was observed on 6 August 2013 at 20:12:22 UTC and has latitudinal extent from 160°E to 162°E. The bottom scene has a lesser degree of convective clustering than the top scene and has a correspondingly lesser mean precipitation rate. Rain type classification is provided by the TRMM-PR dataset (see Materials and Methods). UTC, universal time coordinated.

the Supplementary Materials). For the remainder of this article, unless specified otherwise, results shown use $I_{org}$ computed without grouping of adjacent convective pixels. We refer to the set of choices of scene size, rain rate thresholds, and grouping methods as our "parameter space."

When partitioned into CAF and SF bins (Fig. 2, A to C), the bin-mean precipitation rate shows a clearly increasing trend with both CAF and SF, consistent with previous studies (*13*–*21*). To quantify the effect of mesoscale convective clustering on precipitation rate, for each CAF-SF bin, we subtract the mean precipitation rate of scenes with $I_{org}$values in the first (bottom) quartile from the mean precipitation rate of scenes with $I_{org}$values in the fourth (top) quartile (Fig. 2, D to F). Hereafter, the two groups of scenes are referred to as the weakly clustered and strongly clustered scenes. The most distinctive feature in Fig. 2 (D to F) is that the statistically significant differences are positive for almost every CAF-SF bin, indicating that when CAF and SF are prescribed, enhanced convective clustering results in an increase in precipitation rate over a scene. It is worthwhile to note that our finding is in contrast to recent studies that concluded that domain-averaged precipitation rate is independent of the degree of convective clustering (*13*, *23*). However, while these studies examined how average precipitation rate and average $I_{org}$ vary with quantities similar to CAF and SF, they did not constrain their data by both their CAF and SF proxies. Thus, we argue that our study more fairly compares scenes whose primary difference is in the degree of convective clustering.

The difference in mean $I_{org}$ values between strongly and weakly clustered scenes decreases with CAF (Fig. 2, G to I). This feature is also present across our parameter space (see the Supplementary Materials). This indicates that the sensitivity of domain-mean precipitation to convective clustering is increased when a greater number of convective entities is present, suggesting that convective clustering enhances precipitation rate via self-reinforcing interactions between the convective elements. Such self-reinforcing interactions, such as the moistening of environmental air via detrainment, would have a greater effect on the precipitation rate when CAF is higher than when CAF is lower. Thus, Fig. 2 (G to I) suggests that, over high-CAF scenes, the effects of a small change in the degree of convective clustering are magnified by the fact that more convective elements are present and, thus, their capacity for self-reinforcement is increased.

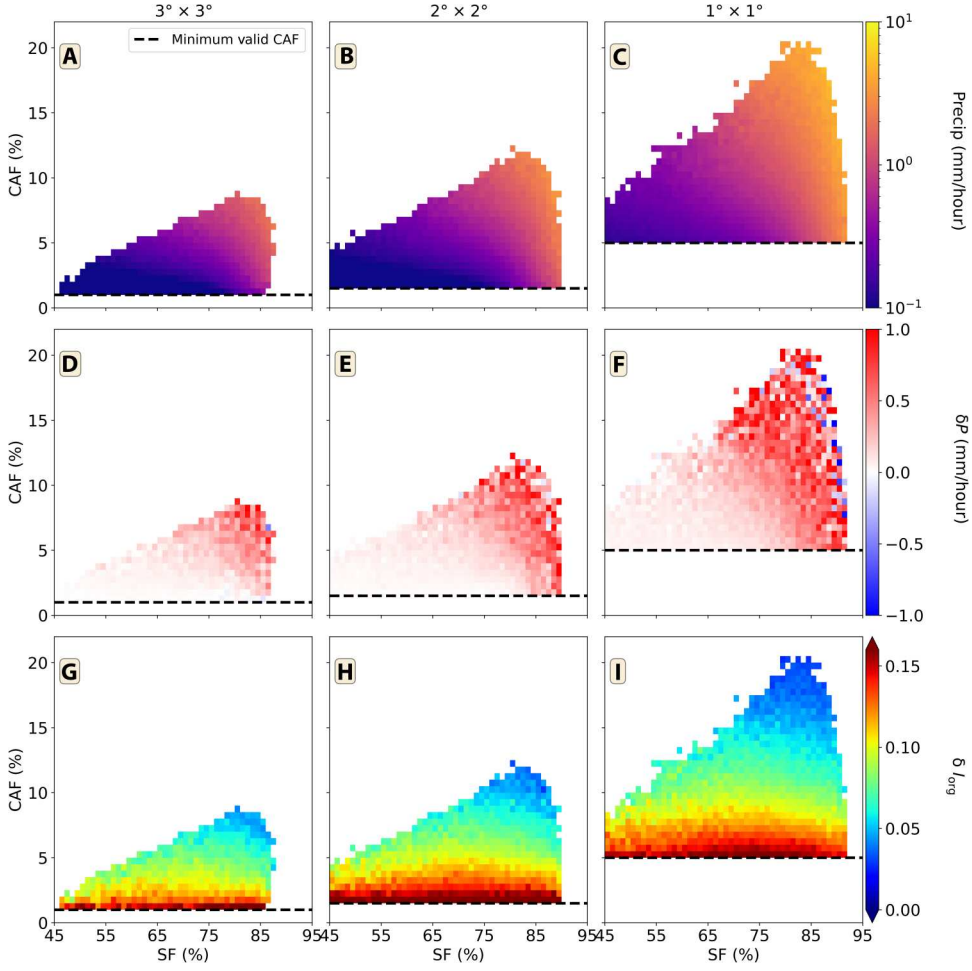


**Fig. 2. Precipitation and $I_{org}$ variability with CAF and SF.** (**A** to **C**) Mean precipitation rate of scenes with given CAF and SF. (**D** to **F**) The difference in average precipitation rate of strongly and weakly clustered scenes. (**G** to **I**) The difference in average $I_{org}$ between strongly and weakly clustered scenes. Results shown in this figure are with $I_{org}$ computed without rain threshold or grouping. Minimum valid CAF is defined as the CAF corresponding to 20 convective pixels (see Materials and Methods).

As a quantitative estimate of the enhancement of precipitation attributable to enhanced mesoscale convective clustering, we define the precipitation enhancement due to mesoscale convective clustering (PEMC) as the percent difference in the mean precipitation intensities between the strongly clustered and weakly clustered scenes

$$\mathrm{PEMC} = \frac{P^{\mathrm{SC}} - P^{\mathrm{WC}}}{P^{\mathrm{WC}}} \times 100\% \quad (1)$$

where $P^{\mathrm{SC}}$ and $P^{\mathrm{WC}}$ are the mean precipitation intensities of the strongly and weakly clustered scenes, respectively. Note that PEMC is computed for each CAF-SF bin. PEMC values for a subset of our parameter space (computed without grouping) are shown in Fig. 3; the results are qualitatively similar across the whole of our parameter space (Figs. S6 and S7). Values shown are statistically significant at the 95th confidence level as determined by a permutation test. The most notable feature of Fig. 3 is that statistically significant PEMC values are positive for almost all CAF-SF bins. Across our parameter space, mean PEMC values range from about 10% to close to 60% (Fig. 4). We observe that both mean PEMC values and PEMC values for individual CAF-SF bins are sensitive to both the size of scene and the choice of how $I_{\mathrm{org}}$ is computed. However, the mean value of PEMC is positive in all cases tested in our parameter space, indicating the robustness of our finding that mesoscale convective clustering enhances precipitation.

## Convective clustering does not affect convective-stratiform partitioning

To diagnose the contributions of convective and stratiform processes to the enhancement of precipitation associated with a stronger degree of mesoscale convective clustering, we decompose the precipitation intensity over a scene as

$$P = P_c a_c + P_s a_s \quad (2)$$

where $P_c$ and $P_s$ are the conditional convective and stratiform precipitation intensities and $a_c$ and $a_s$ are the CAF and stratiform area fraction, respectively (see Materials and Methods). For each CAF-SF bin, $P^{\mathrm{SC}}$ and $P^{\mathrm{WC}}$ are related by

$$P^{\mathrm{SC}} = P^{\mathrm{WC}} + \delta P \quad (3)$$

where $\delta P$ is the increase in rain rate between weakly and strongly clustered scenes. We can combine Eqs. 2 and 3 and use the fact that PEMC = $\delta P/P^{\mathrm{WC}}$ to write PEMC as the sum of four terms and ascribe meaning to each

$$\mathrm{PEMC} = \underbrace{\frac{a_c^{\mathrm{WC}}\delta P_c}{P^{\mathrm{WC}}}}_{\substack{\text{Convective}\\ \text{precipitation}\\ \text{enhancement}}} + \overbrace{\frac{a_s^{\mathrm{WC}}\delta P_s}{P^{\mathrm{WC}}}}^{\substack{\text{Stratiform}\\ \text{precipitation}\\ \text{enhancement}}} + \underbrace{\frac{P_s^{\mathrm{WC}}\delta a_s}{P^{\mathrm{WC}}}}_{\substack{\text{Stratiform area}\\ \text{enhancement}}} + \overbrace{\frac{\delta P_s \delta a_s}{P^{\mathrm{WC}}}}^{\text{Covariance}} \quad (4)$$

where $\delta X$ is the difference in the mean values of $X$ between the strongly and weakly clustered scenes (where $X = P_c$, $P_s$, $a_c$,or $a_s$). Equation 4 thus provides a framework to diagnose the contribution of individual processes to the enhancement of precipitation. Note that since PEMC is defined for each CAF-SF bin, the contribution to PEMC associated with changes in convective area is negligible and thus not included in Eq. 4.

Figure 5 (A to I) shows the first three terms in Eq. 4; the covariance term is negligibly small for every CAF-SF bin. In the regime SF $\lesssim$ 70%, the dominant contribution to PEMC is from the strengthening of convective precipitation. When SF $\gtrsim$ 70%, on the other hand, the enhancement of precipitation resulting from an enhancement of stratiform area fraction increases to a level comparable to the enhancement of convective precipitation and eventually becomes dominant when SF $\gtrsim$ 80%. This transition can be more clearly seen in Fig. 5 (J to L), in which the latter three terms of Eq. 4 are combined into a stratiform component of enhancement, and a convective component of enhancement is similarly defined as the remaining term of Eq. 4. The convective and stratiform components of enhancement are expressed as a percentage of PEMC to quantify their contribution to the total precipitation enhancement. As shown in Fig. 5 (J to L), the stratiform component of enhancement is the dominant component for SF values greater than about 85%.

The transition of PEMC from being dominated by its convective component when SF is low to being comprised by its convective and stratiform components in about equal measure at higher SF (with the stratiform component eventually being dominant at very high SF) is reminiscent of the fact that stratiform precipitation occurs almost exclusively in environments with SF > 70% (*20*, *21*). This suggests that, for a given SF, the relative importance of PEMC′s convective and stratiform components is set by the relative frequency of convective and stratiform precipitation at that SF. That is, at a given SF, the fraction of total precipitation that is convective or stratiform is largely determined by the SF of the environment; mesoscale convective clustering increases the total amount of precipitation but does not substantially alter the partition between convective and stratiform precipitation.

To verify this hypothesized invariance of the convective/stratiform partition, we compare the convective rain fraction (CRF) and stratiform rain fraction (SRF) of strongly and weakly clustered scenes, averaged over each CAF bin with a statistically significant value of PEMC (computed without grouping; Fig. 6). CRF decreases with SF for both weakly and strongly clustered scenes, while SRF increases with SF, in agreement with previous studies (*20*, *21*). We can further see that CRF and SRF differ only marginally between strongly and weakly clustered scenes, indicating that mesoscale convective clustering does not significantly alter the partition between convective and stratiform elements. We can see that in the range of 60% < SF < 80%, there is a slight but notable difference in CRF and SRF between strongly and weakly clustered scenes; in this SF range, strongly clustered scenes have a greater CRF (and thus lesser SRF) than weakly clustered scenes, indicating that strongly clustered scenes experience more intense convective precipitation than weakly clustered scenes. Notably, a corresponding increase in SRF for SF > 85%, where the stratiform component of PEMC becomes dominant, is not evident in Fig. 6.

As evidenced by Fig. 6, the CRF and SRF of a scene are primarily functions of SF and are only slightly modified by the presence of strong convective clustering. Thus, the fact that PEMC′s stratiform component becomes comparable in magnitude to its convective component near SF $\approx$ 70% is a consequence of the invariance of CRF (and SRF) to the degree of convective clustering: as SF increases, SRF increases, and thus, the stratiform component of PEMC

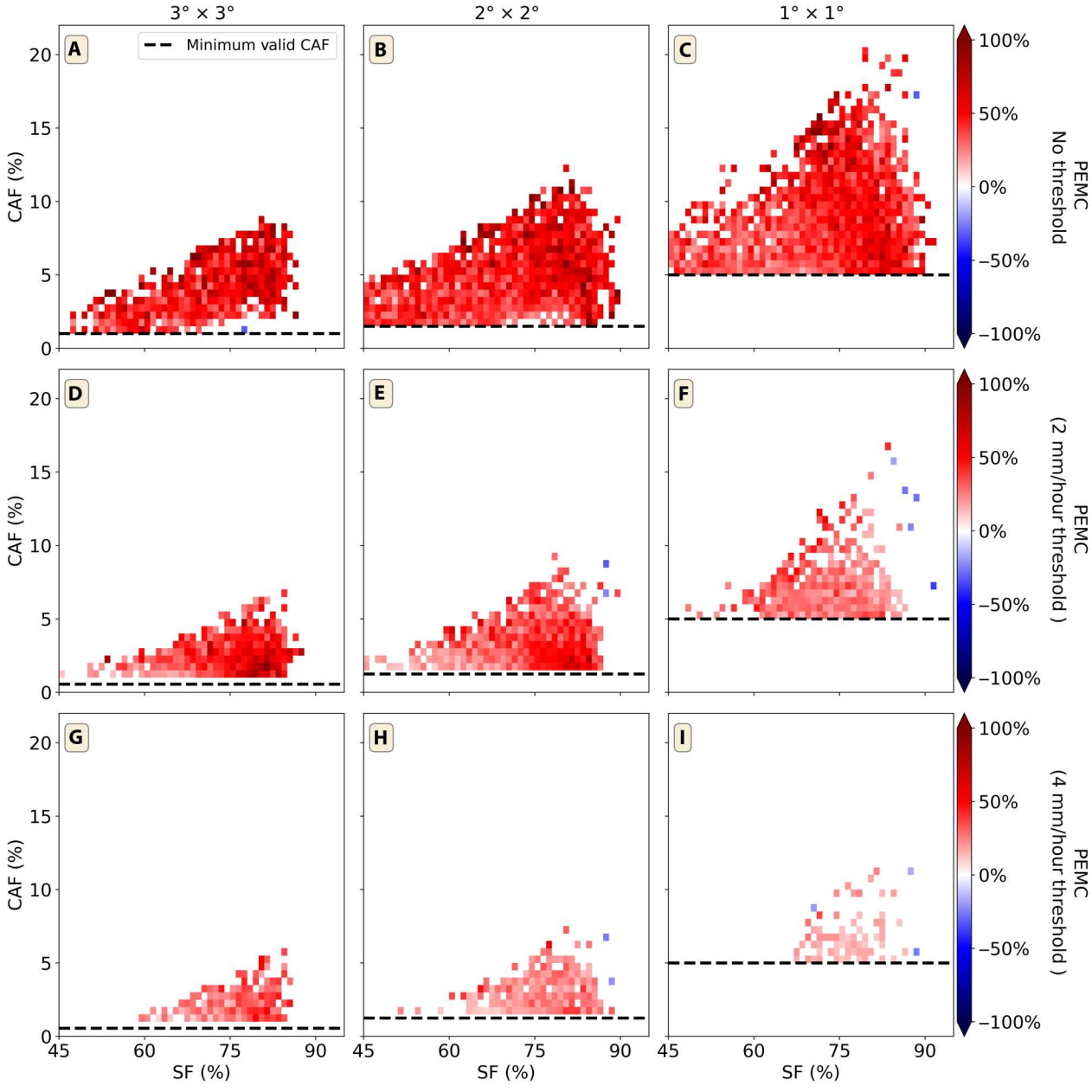


**Fig. 3. PEMC.** Values shown are statistically significant at the 95th confidence level as determined by a permutation test. The $I_{org}$ values used in identifying strongly and weakly clustered scenes were computed (**A** to **C**) with no threshold, (**D** to **F**) with a 2 mm/hour precipitation rate threshold, (**G** to **I**) and with 4 mm/hour precipitation rate threshold (see Materials and Methods).

increases in proportion. Note that CRF is not completely ambivalent to the degree of convective clustering for scenes with 60% < SF < 80%, as evidenced by the slightly greater CRF in strongly clustered scenes than in weakly clustered scenes in this range. If we assume that mesoscale convective clustering enhances convective strength via a moistening of the environment, as suggested by numerous prior studies (*27*–*30*), then we may also put forth an explanation to the fact that strongly and weakly clustered scenes have a different CRF in the range of 60% < SF < 80%. Below this range, the environment is too subsaturated to sustain deep convection, regardless of the degree of convective clustering; above this range, the environment is already sufficiently moist that increasing the degree of clustering has no meaningful impacts on precipitation. Thus, convective clustering is most effective in increasing CRF when the environment is moist enough to sustain convection but not so moist that convective clustering has little effect on convective strength.

## DISCUSSION

This study has estimated the enhancement of precipitation that occurs as a result of convective clustering per se, controlling for

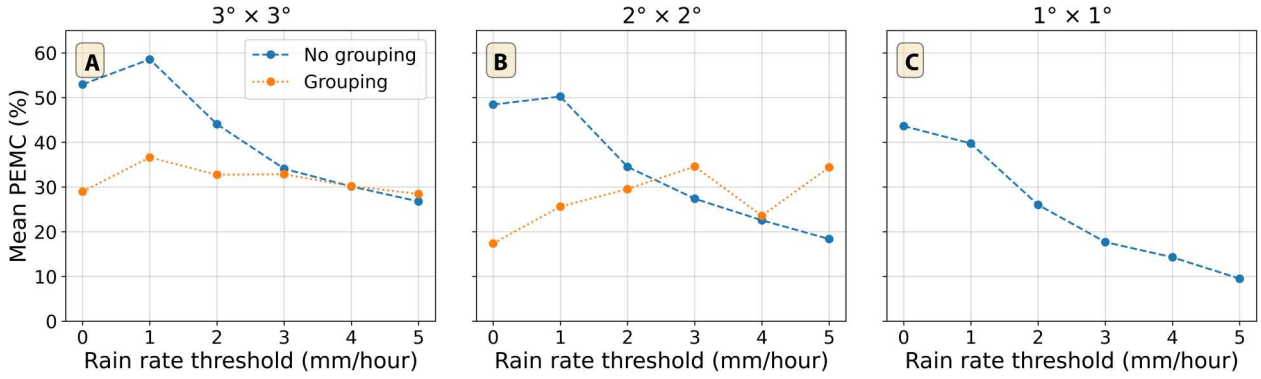


**Fig. 4. Sensitivity of PEMC.** The mean value of statistically significant PEMC values, as computed with and without grouping of connected convective pixels, and with indicated rain rate thresholds, for (**A**) 3° × 3° scenes, (**B**) 2° × 2° scenes, (**C**) and 1° × 1° scenes. Note that no $I_{org}$ values can be computed for 1° × 1° scenes with grouping of adjacent convective pixels (see Materials and Methods).

the enhancement resultant from an increase in environmental column moisture and CAF. The enhancement factor (Fig. 3) and its partitioning into convective and stratiform processes (Fig. 5) can serve as an observational reference against which the performance of various modeling systems may be assessed. As shown in Fig. 4, the exact value of PEMC is sensitive to the spatial size of the domain, as well as rain rate thresholds or choice of grouping method used when quantifying the degree of clustering via $I_{org}$. Model resolution and differences in how convective elements are identified should therefore be considered when making comparisons to the present study. With the fast advances being made in the numerical modeling of weather and climate, including global storm-permitting models (*31*), such an observational benchmark will be of great utility in evaluating the realism of the models′ representations of mesoscale systems of clustered convection. These diagnostic appraisals of model realism will aid in the forecasting of extreme precipitation and help constrain predicted global warming–driven changes to precipitation patterns.

## MATERIALS AND METHODS

### Precipitation and CAF

Scene-averaged precipitation and CAF data are obtained from the NASA TRMM-PR dataset (*32*). The data used are derived from two TRMM-PR version 7 products: 2A23 precipitation radar rain characteristics (*33*, *34*), which classifies observed rainfall as convective, stratiform, or other, and 2A25 precipitation radar echo data (*35*), which provides attenuation-corrected radar reflectivity. Pixels labeled as other contribute a negligible amount to the total precipitation observed by TRMM, so that rainy pixels can be safely thought of as being either convective or stratiform. All these data have instantaneous time resolution. The TRMM data are interpolated onto a regular 0.05° × 0.05° grid of pixels.

The data used are composed of a set of snapshots made up of gridded pixels. Each pixel provides surface rain rate and rain type data. Each snapshot is portioned into several nonoverlapping scenes. Since the satellite′s observational swath does not, in general, completely cover a given scene, only those scenes with more than 70% of its area covered by the observational swath are considered in our study. This ensures that each scene is adequately sampled to estimate its mean properties. Each pixel may be referred to its rain type label (e.g., a pixel recorded as undergoing convective precipitation).

Scenes are collected from four 40° × 30° regions, chosen to represent major tropical oceanic basins: the western Pacific Ocean, bounded by 150°E to 190°E; the eastern Pacific Ocean, bounded by 160°W to 120°W; the tropical Atlantic Ocean, bounded by 41°W to 1°W; and the central Indian Ocean, bounded by 55°E to 95°E. All regions are bounded meridionally by 15°S to 15°N (fig. S1). The data collected are from 1 January 1998 to 31 December 2013. Only CAF-SF bins with more than 50 constituent scenes are considered in our analysis.

Scene-averaged precipitation rate is computed by dividing the sum of precipitation rates for all pixels in the observational scene by the number of pixels in the swath. This method allows for fair comparisons between scenes with differing swath coverage extents. Conditional convective precipitation and stratiform precipitation intensities ($P_c$ and $P_s$ in Eq. 2) are computed similarly, with convective (stratiform) precipitation rate being defined as the sum of precipitation rate data for all convective (stratiform) pixels divided by the number of convective (stratiform) pixels. CAF ($a_c$ in Eq. 2) and stratiform area fraction ($a_s$ in Eq. 2) are computed as the ratio of the total number of the corresponding type of pixel to the total number of pixels in the swath.

### Saturation fraction

SF data are obtained from the ERA5 global reanalysis dataset produced by the ECMWF (*22*). These data are provided on a global 0.25° × 0.25° grid with hourly resolution. Vertical profiles of both specific humidity and temperature are used to compute saturation-specific humidity profiles via the Clausius-Clapeyron relation. The vertical integrals of specific humidity and saturation-specific humidity are computed from 1000 to 100 hPa and then averaged across the scene. SF is obtained by dividing the mean vertical integral of specific humidity by the mean vertical integral of saturation-specific humidity.

### Organization index

The degree of mesoscale convective clustering is quantified by the organization index ($I_{org}$) (*24*). This index is computed by integrating the cumulative density function of nearest-neighbor distances between convective elements in a scene with respect to the

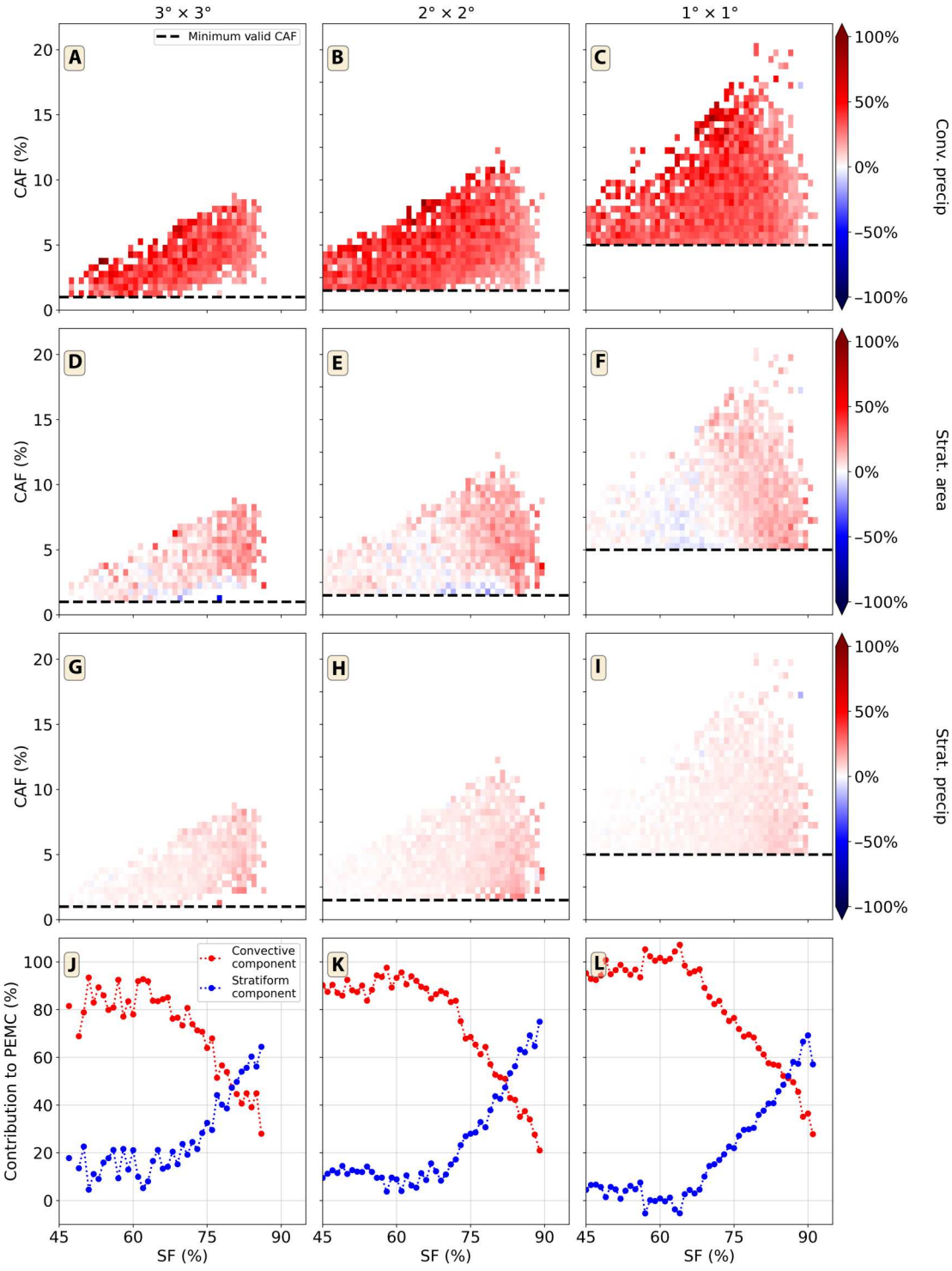


**Fig. 5. Components of PEMC.** The enhancements of (**A** to **C**) convective precipitation rate, (**D** to **F**) stratiform area fraction, (**G** to **I**) and stratiform precipitation rate are computed for each CAF-SF bin, as defined in Eq. 4. (**J** to **L**) The combined stratiform component (latter three terms of Eq. 4) and convective component are averaged over CAF bins. Results shown are with $I_{org}$ computed without rain threshold or grouping.

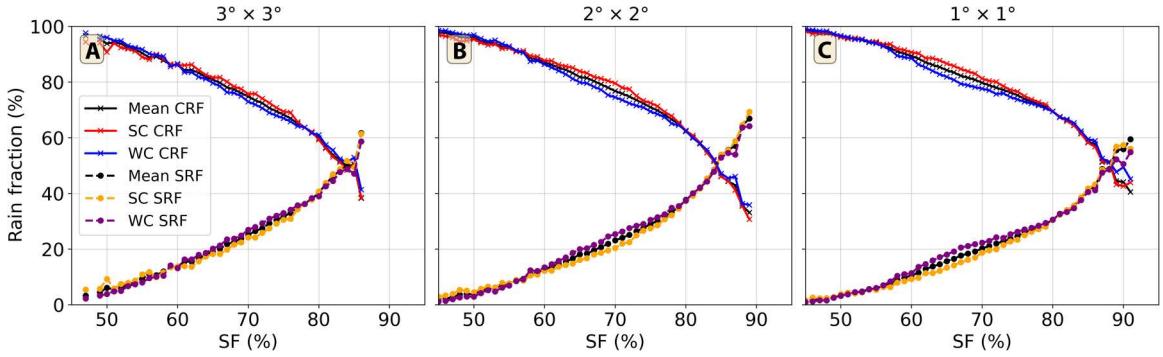


**Fig. 6. CRFs and SRFs.** Average values of the CRFs of strongly clustered scene (SC CRF), CRFs of weakly clustered scenes (WC CRF), SRFs of strongly clustered scene (SC SRF), and SRFs of weakly clustered scenes (WC SRF) are averaged over CAF bins. Results shown are with $I_{org}$ computed without rain threshold or grouping. Results shown for (**A**) 3° × 3° scenes, (**B**) 2° × 2° scenes, and (**C**) 1° × 1° scenes.

distribution that would be expected if the same number of convective elements was randomly distributed about the scene. This integral yields a number between 0 and 1. An $I_{org}$ value less than 0.5 indicates that convection is less clustered than would be expected from a random distribution; an $I_{org}$ value greater than 0.5 indicates that convective elements are more clustered than random.

Some previous studies [e.g., (*13*, *25*)] have computed $I_{org}$ by grouping adjacent convective pixels, with the location of each group of contiguous convective pixels described by its geometric centroid. Since $I_{org}$ is most robust when there are more than 20 convective objects being considered, this method can only be used for 2° × 2° and 3° × 3° scenes; no 1° × 1° scene has 20 or more contiguous convective groups. In addition, some previous studies have used precipitation thresholds to identify convection. To test the sensitivity of our results to these choices in how $I_{org}$ is computed, we perform our analysis by computing $I_{org}$ both with and without grouping adjacent connective pixels; we additionally computed $I_{org}$ with and without precipitation thresholds, where the pixels considered in the computation of $I_{org}$ must both be identified as convective by TRMM and also have precipitation greater than some threshold. Note that these thresholds are not used in the computation of CAF.

### Precipitation enhancement budget

Combining Eqs. 2 and 3, for a given CAF $a_c$ and stratiform area fraction $a_s$, we can write the difference between the mean precipitation of strongly clustered scenes $P^{SC}$ and the weakly clustered scenes $P^{WC}$ as the combination of changes of each of the terms in Eq. 1

$$P^{SC} = (P_c^{WC} + \delta P_c)(a_c^{WC} + \delta a_c) + (P_s^{WC} + \delta P_s)(a_s^{WC} + \delta a_s) \quad \text{(M1)}$$

where $P_c^{WC}$ is the mean convective precipitation rate of weakly clustered scenes and $\delta P_c$ is the difference between $P_c^{WC}$ and the mean convective precipitation rate of strongly organized scenes. The other terms are defined similarly. Note that since $P^{SC}$ and $P^{WC}$ have been defined as being from the same CAF bin, $\delta a_c \approx 0$. We can multiply and group the terms of Eq. M1 to obtain

$$P^{SC} = [P_c^{WC} a_c^{WC} + P_s^{WC} a_s^{WC}] + (a_c^{WC} \delta P_c + a_s^{WC} \delta P_s + P_s^{WC} \delta a_s + \delta P_s \delta a_s) \quad \text{(M2)}$$

We recognize the bracketed quantity as $P^{WC}$, as defined in Eq. 1. It follows then that the parenthetical terms sum together to give $\delta P$, as defined in Eq. 3. Using the fact that PEMC = $\delta P / P^{WC}$, we can divide the parenthetical terms of Eq. M2 by $P^{WC}$ to obtain Eq. 4.

## Supplementary Materials

**This PDF file includes:**

Supplementary Text
Figs. S1 to S9

## REFERENCES AND NOTES


1. R. A. Houze, Jr., Mesoscale convective systems. *Rev. Geophy.* **42**, RG4003 (2004).
2. R. A. Madden, P. R. Julian, Detection of a 40–50 day oscillation in the zonal wind in the tropical pacific. *J. Atmos. Sci.* **28**, 702–708 (1971).
3. S. W. Nesbitt, R. Cifelli, S. A. Rutledge, Storm morphology and rainfall characteristics of TRMM precipitation features. *Mon. Wea. Rev.* **134**, 2702–2721 (2006).
4. L. Jaramillo, G. Poveda, J. F. Mejía, Mesoscale convective systems and other precipitation features over the tropical americas and surrounding seas as seen by TRMM. *Int. J. Climatol.* **37**, 380–397 (2017).
5. R. Roca, T. Fiolleau, Extreme precipitation in the tropics is closely associated with long-lived convective systems. *Commun. Earth Environ.* **1**, 18 (2020).
6. C. Moseley, C. Hohenegger, P. Berg, J. O. Haerter, Intensification of convective extremes driven by cloud–cloud interaction. *Nat. Geosci.* **9**, 748–752 (2016).
7. N. Dai, B. J. Soden, Convective aggregation and the amplification of tropical precipitation extremes. *AGU Adv.* **1**, e2020AV000201 (2020).
8. J. Tan, C. Jakob, W. B. Rossow, G. Tselioudis, Increases in tropical rainfall driven by changes in frequency of organized deep convection. *Nature* **519**, 451–454 (2015).
9. A. G. Pendergrass, Changing degree of convective organization as a mechanism for dynamic changes in extreme precipitation. *Curr. Clim. Change Rep.* **6**, 47–54 (2020).
10. A. G. Pendergrass, K. A. Reed, B. Medeiros, The link between extreme precipitation and convective organization in a warming climate: Global radiative-convective equilibrium simulations. *Geophys. Res. Lett.* **43**, 11445–11452 (2016).
11. C. Rio, A. D. Del Genio, F. Hourdin, Ongoing breakthroughs in convective parameterization. *Curr. Clim. Change Rep.* **5**, 95–111 (2019).
12. B. Mapes, R. Neale, Parameterizing convective organization to escape the entrainment dilemma. *J. Adv. Model. Earth Syst.* **3**, M06004 (2011).
13. M. Brueck, C. Hohenegger, B. Stevens, Mesoscale marine tropical precipitation varies independently from the spatial arrangement of its convective cells. *Q. J. Roy. Meteorol. Soc.* **146**, 1391–1402 (2020).
14. A. Doneaud, S. Ionescu-Niscov, D. L. Priegnitz, P. L. Smith, The area-time integral as an indicator for convective rain volumes. *J. Appl. Meteorol. Climatol.* **23**, 555–561 (1984).
15. L. Davies, C. Jakob, P. May, V. V. Kumar, S. Xie, Relationships between the large-scale atmosphere and the small-scale convective state for Darwin, Australia. *J. Geophys. Res. Atmos.* **118**, 11534–11545 (2013).
16. L. Nuijens, B. Stevens, A. P. Siebesma, The environment of precipitating shallow cumulus convection. *J. Atmos. Sci.* **66**, 1962–1979 (2009).

17. C. S. Bretherton, M. E. Peters, L. E. Back, Relationships between water vapor path and precipitation over the tropical oceans. *J. Climate* **17**, 1517–1528 (2004).
18. S. S. Rushley, D. Kim, C. S. Bretherton, M.-S. Ahn, Reexamining the nonlinear moisture-precipitation relationship over the tropical oceans. *Geophys. Res. Lett.* **45**, 1133–1140 (2018).
19. Á. F. Adames, S. W. Powell, F. Ahmed, V. C. Mayta, J. D. Neelin, Tropical precipitation evolution in a buoyancy-budget framework. *J. Atmos. Sci.* **78**, 509–528 (2021).
20. F. Ahmed, C. Schumacher, Convective and stratiform components of the precipitation-moisture relationship. *Geophys. Res. Lett.* **42**, 10453–10462 (2015).
21. B. Wolding, J. Dias, G. Kiladis, F. Ahmed, S. W. Powell, E. Maloney, M. Branson, Interactions between moisture and tropical convection. Part I: The coevolution of moisture and convection. *J. Atmos. Sci.* **77**, 1783–1799 (2020).
22. H. Hersbach, B. Bell, P. Berrisford, S. Hirahara, A. Horányi, J. Muñoz-Sabater, J. Nicolas, C. Peubey, R. Radu, D. Schepers, A. Simmons, C. Soci, S. Abdalla, X. Abellan, G. Balsamo, P. Bechtold, G. Biavati, J. Bidlot, M. Bonavita, G. De Chiara, P. Dahlgren, D. Dee, M. Diamantakis, R. Dragani, J. Flemming, R. Forbes, M. Fuentes, A. Geer, L. Haimberger, S. Healy, R. J. Hogan, E. Hólm, M. Janisková, S. Keeley, P. Laloyaux, P. Lopez, C. Lupu, G. Radnoti, P. de Rosnay, I. Rozum, F. Vamborg, S. Villaume, J.-N. Thépaut, The ERA5 global reanalysis. *Q. J. Roy. Meteorol. Soc.* **146**, 1999–2049 (2020).
23. A. G. Semie, S. Bony, Relationship between precipitation extremes and convective organization inferred from satellite observations. *Geophys. Res. Lett.* **47**, e2019GL086927 (2020).
24. A. M. Tompkins, A. G. Semie, Organization of tropical convection in low vertical wind shears: Role of updraft entrainment. *J. Adv. Model. Earth Syst.* **9**, 1046–1068 (2017).
25. W.-Y. Cheng, D. Kim, A. Rowe, Objective quantification of convective clustering observed during the AMIE/DYNAMO two-day rain episodes. *J. Geophys. Res. Atmos.* **123**, 10361–10378 (2018).
26. A. A. Wing, C. L. Stauffer, T. Becker, K. A. Reed, M.-S. Ahn, N. P. Arnold, S. Bony, M. Branson, G. H. Bryan, J.-P. Chaboureau, S. R. De Roode, K. Gayatri, C. Hohenegger, I.-K. Hu, F. Jansson, T. R. Jones, M. Khairoutdinov, D. Kim, Z. K. Martin, S. Matsugishi, B. Medeiros, H. Miura, Y. Moon, S. K. Müller, T. Ohno, M. Popp, T. Prabhakaran, D. Randall, R. Rios-Berrios, N. Rochetin, R. Roehrig, D. M. Romps, J. H. Ruppert Jr., M. Satoh, L. G. Silvers, M. S. Singh, B. Stevens, L. Tomassini, C. C. van Heerwaarden, S. Wang, M. Zhao, Clouds and convective self-aggregation in a multimodel ensemble of radiative-convective equilibrium simulations. *J. Adv. Model. Earth Syst.* **12**, e2020MS002138 (2020).
27. W. M. Hannah, Entrainment versus dilution in tropical deep convection. *J. Atmos. Sci.* **74**, 3725–3747 (2017).
28. T. Becker, C. S. Bretherton, C. Hohenegger, B. Stevens, Estimating bulk entrainment with unaggregated and aggregated convection. *Geophys. Res. Lett.* **45**, 455–462 (2018).
29. Z. Feng, S. Hagos, A. K. Rowe, C. D. Burleyson, M. N. Martini, S. P. de Szoeke, Mechanisms of convective cloud organization by cold pools over tropical warm ocean during the AMIE/DYNAMO field campaign. *J. Adv. Model. Earth Syst.* **7**, 357–381 (2015).
30. D. H. Moser, S. Lasher-Trapp, S., Cloud-spacing effects upon entrainment and rainfall along a convective line. *J. Appl. Meteorol. Climatol.* **57**, 1865–1882 (2018).
31. B. Stevens, M. Satoh, L. Auger, J. Biercamp, C. S. Bretherton, X. Chen, P. Düben, F. Judt, M. Khairoutdinov, D. Klocke, C. Kodama, L. Kornblueh, S.-J. Lin, P. Neumann, W. M. Putman, N. Röber, R. Shibuya, B. Vanniere, P. L. Vidale, N. Wedi, L. Zhou, DYAMOND: The DYnamics of the atmospheric general circulation modeled on non-hydrostatic domains. *Prog Earth Planet Sci* **6**, 61 (2019).
32. R. A. Houze Jr., K. L. Rasmussen, M. D. Zuluaga, S. R. Brodzik, The variable nature of convection in the tropics and subtropics: A legacy of 16 years of the tropical rainfall measuring mission satellite. *Rev. Geophys.* **53**, 994–1021 (2015).
33. J. Awaka, T. Iguchi, K. Okamoto, TRMM PR standard algorithm 2A23 and its performance on bright band detection. *J. Meteorol. Soc. Japan* **87A**, 31–52 (2009).
34. Tropical Rainfall Measuring Mission (TRMM), TRMM Precipitation Radar Rain Characteristics L2 1.5 hours V7 (Goddard Earth Sciences Data and Information Services Center, 2011).
35. Tropical Rainfall Measuring Mission (TRMM), TRMM Precipitation Radar Rainfall Rate and Profile L2 1.5 hours V7 (Goddard Earth Sciences Data and Information Services Center, 2011).

**Acknowledgments**
**Funding:** D.K. and P.A.-U. were supported by the National Aeronautics and Space Administration grant 80NSSC17K0227 (to P.A.-U. and D.K.), National Oceanic and Atmospheric Administration grant NA18OAR4310276 (to D.K.), National Oceanic and Atmospheric Administration grant NA18OAR4310300 (to D.K.), Department of Energy grant DE-SC0016223 (to D.K.), Korea Meteorological Administration Research and Development program under grant KMI2021-01210 (to D.K.), and Korea National Research Foundation Brain Pool program under grant NRF-2021H1D3A2A01039352 (to D.K.). **Author contributions:** Conceptualization: D.K. Methodology: P.A.-U. and DK. Investigation: P.A.-U. and D.K. Visualization: P.A.-U. Supervision: D.K. Writing—original draft: P.A.-U. and D.K. Writing—review and editing: P.A.-U. and D.K. **Competing interests:** The authors declare that they have no competing interests. **Data and materials availability:** All data needed to evaluate the conclusions in the paper are present in the paper and/or the Supplementary Materials. In addition, the raw TRMM rain rate and rain type data are available at http://trmm.atmos.washington.edu. The moisture, organization, and convective population metrics of each scene analyzed in the paper are available at https://doi.org/10.5281/zenodo.6655261.

Submitted 10 February 2022
Accepted 13 December 2022
Published 11 January 2023
10.1126/sciadv.abo5317